JOURNAL OF CATALYSIS 154, 253–260 (1995)

On the Role of the $VO(H_2PO_4)_2$ Precursor for *n*-Butane Oxidation into Maleic Anhydride

M. T. Sananes,*,† G. J. Hutchings,† and J. C. Volta*

*Institut de Recherches sur la Catalyse, CNRS, 2 Avenue A. Einstein, 69626, Villeurbanne Cédex, France; and †Leverhulme Centre for Innovative Catalysis, Department of Chemistry, University of Liverpool, P.O. Box 147, Liverpool, L69 3BX, United Kingdom

Received October 24, 1994; revised March 16, 1995

The catalytic role of $VO(H_2PO_4)_2$, the precursor of the $VO(PO_3)_2$ phase, has been studied for *n*-butane oxidation to maleic anhydride. By comparison with the activated VPO catalyst, derived from the $VOHPO_4 \cdot 0.5H_2O$ precursor phase, $VO(H_2PO_4)_2$ gives a highly selective final catalyst. The total oxidation products CO and CO_2 are not observed under any of the conditions examined, a result confirmed by extensive catalyst testing and carbon mass balances. The final catalyst derived from $VO(H_2PO_4)_2$ has a low surface area, ca. 1 m^2/g, and consequently demonstrates low specific activity on the basis of *n*-butane conversion per unit mass. However, the intrinsic activity (activity per unit surface area) is found to be higher than that for catalysts derived from $VOHPO_4 \cdot 0.5H_2O$. Since some $VO(H_2PO_4)_2$ is present in $VOHPO_4 \cdot 0.5H_2O$, which is the precursor of the industrial catalyst, the results of this study complicate the simple model in which the $(VO)_2P_2O_7$ phase derived from $VOHPO_4 \cdot 0.5H_2O$ is responsible for the selective oxidation of *n*-butane. The observation that the precursor $VO(H_2PO_4)_2$ can generate catalysts of high specific activity and of total selectivity to partial oxidation products might provide a useful insight into the design of a new series of high activity and high selectivity partial oxidation catalysts. © 1995 Academic Press, Inc.

INTRODUCTION

The conversion of *n*-butane to maleic anhydride represents the only industrial process for the selective oxidation of alkanes (1, 2). Industrial catalysts are based on the vanadium–phosphorus oxides (VPO). Vanadyl pyrophosphate $(VO)_2P_2O_7$ (V^{4+} phase with a P/V ratio of 1) is considered to be the main crystalline phase for catalysts that are active for *n*-butane oxidation (3). However, the exact nature of the catalytic surface is still a matter for discussion due not only to the difficulty of characterization of the catalyst, but also to the particular conditions of preparation of the VPO precursor. Indeed, whatever the nature of the chemical reagents considered, an excess of phosphorus over vanadium that corresponds to a bulk P/V ratio higher than 1 (4–7) is generally used. In previous studies, the VPO precursor compound is $VOHPO_4 \cdot 0.5H_2O$, which transforms to $(VO)_2P_2O_7$ via a topotactic transformation during the activation of the catalyst (8, 9). The P/V atomic ratio on the surface of the active vanadyl pyrophosphate catalysts has been studied by several authors, using X-ray photoelectron spectroscopy (10–14). A significant phosphorus enrichment has been observed, which was confirmed by SIMS (15). Various potential precursor phases of the vanadium phosphate catalysts have been identified (10). Among these precursor phases, $VO(H_2PO_4)_2$, sometimes referred to as the E phase (2, 3) (with a bulk P/V ratio of 2), has been noted. On calcination, this phase transforms to $VO(PO_3)_2$ (10, 16). Previous studies (10, 17–20) have shown that the particular conditions for the preparation of the $VOHPO_4 \cdot 0.5H_2O$ precursor also favor the presence of $VO(H_2PO_4)_2$, particularly the use of reducing agent in aqueous medium, e.g., HCl (20) or N_2H_4 (10). Furthermore, it is considered that the decomposition of $VO(H_2PO_4)_2$ to $VO(PO_3)_2$, which occurs at a lower temperature than the decomposition of $VOHPO_4 \cdot 0.5H_2O$ to $(VO)_2P_2O_7$, impedes the attainment of a high-surface-area catalyst (20). Indeed, removal of $VO(H_2PO_4)_2$ by a simple solvent extraction method (17) results in a catalyst with an increased surface area. The extraction of $VO(H_2PO_4)_2$ was used by some authors to discriminate between the catalytic roles of the $VO(H_2PO_4)_2$ and $VOHPO_4 \cdot 0.5H_2O$ precursors (21). It was concluded that the amorphous phase with bulk P/V ratio 2.0 derived from the decomposition of $VO(H_2PO_4)_2$ gave almost the same selectivity and activity per unit area for maleic anhydride formation compared to the untreated catalyst composed of a mixture of the amorphous $VO(PO_3)_2$ phase and the crystallized $(VO)_2P_2O_7$ phase. However, other studies (16) consider $VO(PO_3)_2$ to be a less active phase than $(VO)_2P_2O_7$. To date, the catalytic behavior of $VO(PO_3)_2$ has not been discussed and thus it is now the aim of this paper.

In this publication, we describe the catalytic performance and characterization of four VPO catalysts derived

0021-9517/95 $12.00

via activation of the $VO(H_2PO_4)_2$ phase under various controlled conditions.

EXPERIMENTAL

Preparation of the Precursor and of the Catalysts

Pure $VO(H_2PO_4)_2$ was prepared as previously described (22). V_2O_4 (10 g) was refluxed with 85% H_3PO_4 (82 cm^3) (P/V = 10) at 180°C for 1 h. The solution was then evaporated and the precipitate was washed with water and acetone to remove the unreacted H_3PO_4. The solid was dried at 110°C for 15 h.

Three different $VO(PO_3)_2$ catalysts, C1, C2, and C3, were prepared by calcination of the $VO(H_2PO_4)_2$ precursor at 500°C for 24 h under different gaseous atmospheres. Catalyst C1 was obtained by heating in air under previous published conditions (22), while C2 was obtained by heating under nitrogen, and C3 was heated under the atmosphere used in catalytic studies (1.5% *n*-butane in air) (23).

Precursor and Catalyst Characterization

X-ray diffraction patterns of the materials were recorded with a Siemens diffractometer with Cu*Kα* radiation. Raman studies were performed on a Dilor Omars 89 spectrophotometer equipped with an intensified photodiode array detector. The 514.5-nm emission line from an Ar^+ ion laser (Spectra Physics, Model 164) was used for excitation. Due to the low intensity of the obtained spectra, the power of the incident beam on the sample was 200 mW. To reduce both thermal degradation and photodegradation of the samples, the laser beam was scanned on the sample surface by means of a rotating lens. The time of acquisition was 5 s and 100 spectra were accumulated for each spectrum in order to improve the signal-to-noise ratio. The wavenumber values obtained from the spectra were accurate to within about 2 cm^{-1}. The scattered light was collected in the backscattering geometry.

The ^{31}P NMR experiments were performed on a Bruker MSL 300 NMR spectrometer. Conventional spectra were obtained at 121.5 MHz using a 90°*x*-(acquire) sequence. The 90° pulse was 4.2 μs and the delay time between two consecutive scans was 10 s. Samples were typically spun at 4 kHz in zirconia rotors using a double-bearing probehead. The ^{31}P spin-echo spectra were recorded under static conditions, using a $90°x-\tau-180°y-\tau$-(acquire sequence). The 90° pulse was 4.2 μs and τ was 20 μs. For each sample, the irradiation frequency was varied in increments of 100 kHz above and below the ^{31}P resonance of H_3PO_4. The number of spectra thus recorded was dictated by the frequency limits beyond which no spectral intensity was visible. The ^{31}P NMR spin-echo mapping information was then obtained by the juxtaposition of each experimental spectrum.

Surface area was determined by the BET method. Chemical analysis results were obtained by complete dissolution with a sulfuric acid–nitric acid mixture. P was analyzed by molecular absorption and V by atomic absorption. Thermal analysis of the precursor $VO(H_2PO_4)_2$ was performed by decomposition under vacuum with simultaneous analysis of evolved gas by mass spectrometry.

X-ray photoelectron spectroscopy analysis (XPS) was performed with a Hewlett–Packard 5950 interfaced to a data system which allowed the accumulation of spectra. The spectrometer was equipped with an aluminium anode (AlK_α = 1486.6 eV) and O_{1s} binding energies were referenced to the C_{1s} line at 284.5 eV.

Catalytic Testing

The oxidation of *n*-butane was carried out using a microreactor working under varied conditions with 1 cm^3 of the precursor and the feedstock composition $C_4H_{10}/O_2/He$ = 1.5/18.5/80, GSHV = 1000 h^{-1}. Maleic anhydride (MA) and furan were the main products detected, together with traces of acrylic acid. The detection of reactants and products was performed on line using three gas chromatographs: a FID detector for analysis of oxygenates and hydrocarbons on Porapak Q (2 m, 200°C), a FID detector for analysis of hydrocarbons on Porasil C (4 m, 60°C), and a TCD detector for analysis of CO, CO_2, and O_2 (4 m, 100°C). The limit of detection for CO_x was less than 0.1%. Helium was used as the carrier gas. Satisfactory carbon mass balances were obtained for all data presented (98–100%).

RESULTS

Characterization of the Precursor

The XRD spectrum of the precursor is shown in Fig. 1. Figure 2 presents the LRS spectrum recorded at room temperature in the 800–1200 cm^{-1} range, which is related

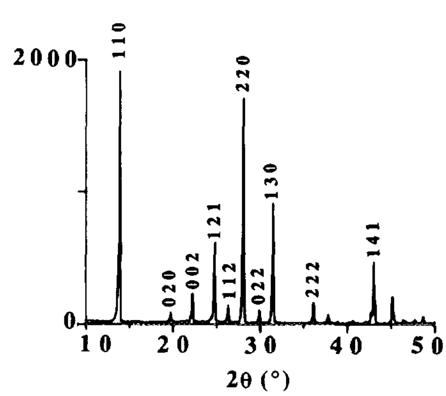

FIG. 1. XRD spectrum of the $VO(H_2PO_4)_2$ precursor.

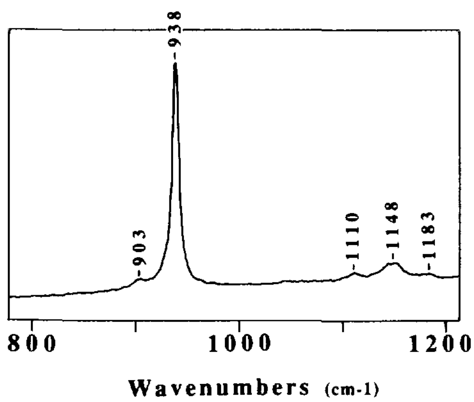

FIG. 2. LRS spectrum of the $VO(H_2PO_4)_2$ precursor.

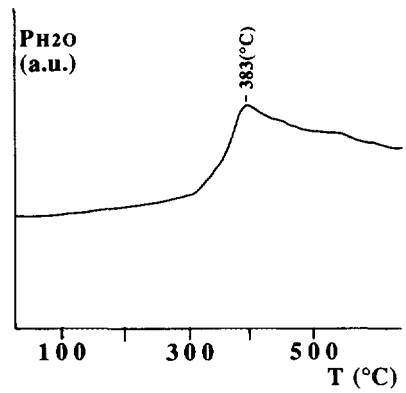

FIG. 4. Water evolution due to decomposition of the $VO(H_2PO_4)_2$ precursor under vacuum.

to the stretching modes of the P–O and V–O bonds (24). No signal was detected by ^{31}P MAS-NMR for this material. The ^{31}P NMR spectrum by spin-echo mapping of the precursor is given in Fig. 3. Figure 4 shows the evolution of water analyzed by mass spectrometry when the precursor is heated under vacuum from room temperature to 650°C at a temperature increase of 2°C/min.

Catalytic Performance

The materials were tested for *n*-butane oxidation in the temperature range 390–410°C, where VPO catalysts derived from the activation of $VOHPO_4 \cdot 0.5H_2O$ give mainly maleic anhydride, CO, and CO_2. It is very interesting to observe that in all the catalysts tested, CO and CO_2 were not detected and only maleic anhydride and furan were observed. This result was confirmed by several repeat experiments. The information is given (Table 1) for *n*-butane conversion (C%), selectivity to maleic anhydride (S_{MA}%), furan (S_{Fur}%), and MA yield (Y_{MA}%). The results obtained from $VO(H_2PO_4)_2$ (E phase) and catalysts C1, C2, and C3 are compared with two VPO catalysts VP(A) and VP(O), derived from $VOHPO_4 \cdot 0.5H_2O$ (26), tested under the same catalytic conditions. The activity is expressed per meter squared (intrinsic activity, IA) and per gram of catalyst (specific activity, SA).

Characterization of the Catalysts after Activation and Catalytic Testing

The X-ray diffraction pattern of the three catalysts C1, C2, and C3 obtained after calcination of the $VO(H_2PO_4)_2$ precursor at 500°C for 24 h in air, under nitrogen, and under 1.5% *n*-butane in air, respectively, are given in Fig. 5. The corresponding LRS and ^{31}P NMR spectra obtained-

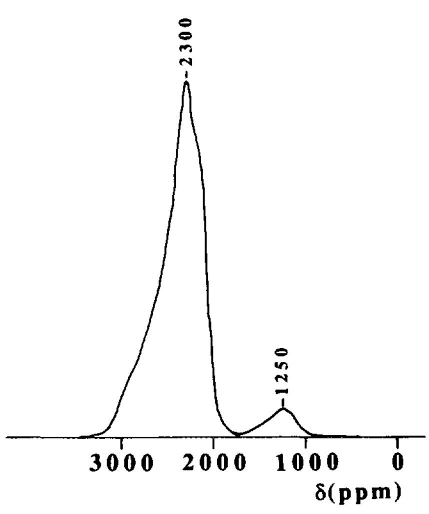

FIG. 3. ^{31}P NMR spectrum by spin-echo mapping of the $VO(H_2PO_4)_2$ precursor.

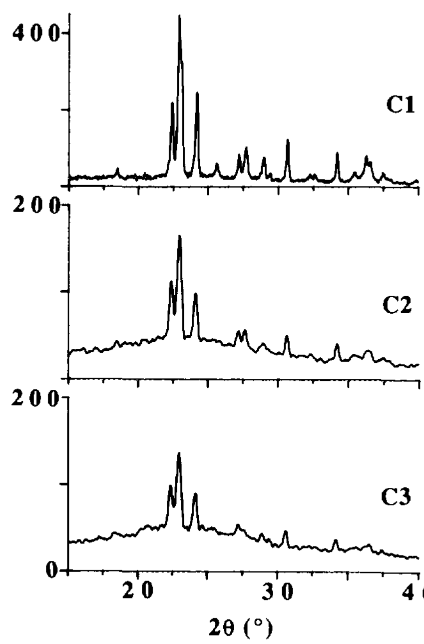

FIG. 5. X-ray spectra of C1, C2, and C3 catalysts after calcination.

TABLE 1

Catalytic Results for *n*-Butane Oxidation at 390°C

Catalyst	C (%)	S_{MA} (%)	S_{Fur} (%)	S_{CO}[a] (%)	S_{CO_2}[a] (%)	Y_{MA} (%)	IA × 10^5 (mol · MA/m^{-2}h^{-1})	SA × 10^5 [b] (mol · MA/g.h)
E	8	75	25	0	0	6.0	2.90	2.90
C1	2	60	40	0	0	1.2	0.94	0.94
C2	6	80	20	0	0	4.8	3.80	3.80
C3	1	100	—	0	0	1.0	1.27	1.27
VP(A)	11	51	—	41	7	5.6	1.24	4.96[c]
VP(O)	27	52	—	34	14	14.0	1.35	18.90[c]

Note. Precursor of VP(A) was prepared by dissolving V_2O_5 (6.06 g) in aqueous HCl (35%, 79 ml) at reflux for 2 h. H_3PO_4 (8.91 g, 85%) was added and the solution was refluxed for another 2 h. The solution was then evaporated to dryness and the resulting solid was refluxed in water (20 ml H_2O/g solid) for 1 h, filtered hot, washed with warm water, and dried in air (110°C, 16 h). The precursor of VP(O) was prepared by adding V_2O_5 (11.8 g) to isobutanol (250 ml); H_3PO_4 (16.49 g, 85%) was introduced to the mixture which was then refluxed for 16 h. The light blue suspension was then separated from the organic solution by filtration and washed with isobutanol (200 ml) and ethanol (150 ml, 100%). The resulting solid was refluxed in water (9 ml H_2O/g solid), filtered hot, and dried in air (110°C, 16 h).

[a] Limit of TCD detection <0.1%.

[b] S_{BET} for all the solids were 1 m^2/g.

[c] See Table 1 in Ref. (26): S_{BET} VP(A) = 4 m^{2}g^{-1} and VP(O) = 14 m^{2}g^{-1}; VP(A) and VP(O) were called C1 and C2, respectively, in Ref. (26).

by spin-echo mapping are shown in Figs. 6 and 7 respectively.

The X-ray diffraction pattern, LRS, and ^{31}P spin-echo mapping NMR spectra of the catalyst derived for the catalytic testing of the E phase at 390–410°C under a butane/air atmosphere are shown in Figs. 8, 9, and 10, respectively. This material differs from catalysts C1, C2, and C3 by virtue of the different calcination conditions. The result for phase E can be compared with catalyst C3 in Figs. 5, 6, and 7.

The ^{31}P spin-echo mapping NMR spectra of catalysts C1, C2, and C3 after catalytic testing are shown in Fig. 11 and they can be compared with the spectra of Fig. 7 for the same materials before reaction.

The results of X-ray photoelectron spectroscopy of phase E and also of phases E and C1 after catalytic testing

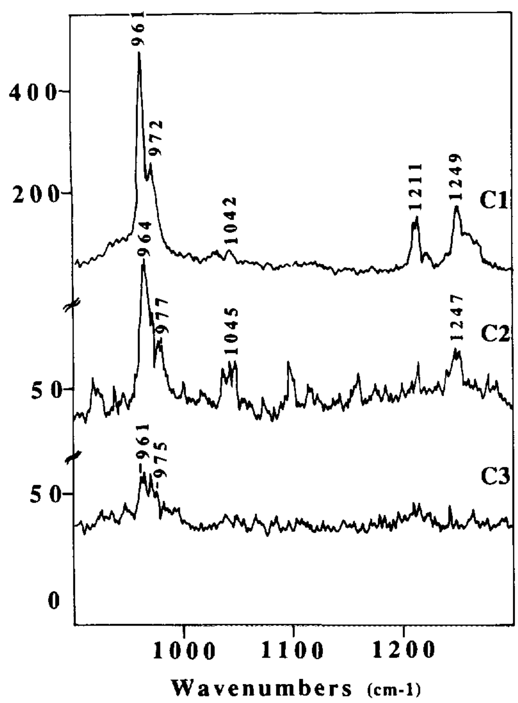

FIG. 6. LRS spectra of C1, C2, and C3 catalysts after calcination.

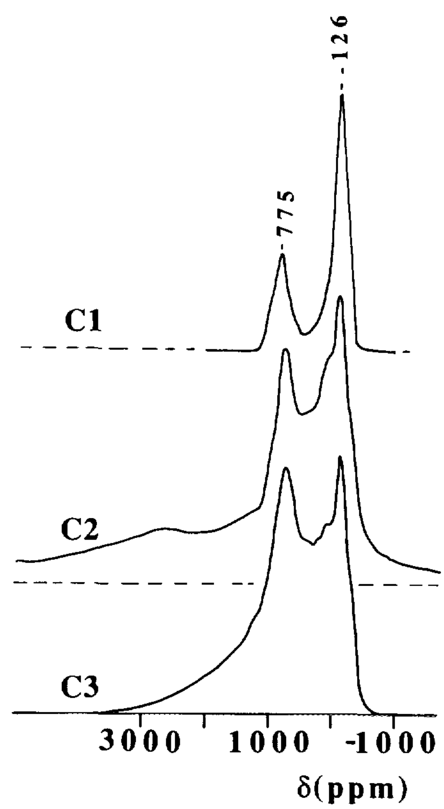

FIG. 7. ^{31}P NMR spectra by spin-echo mapping of C1, C2, and C3 catalysts after calcination.

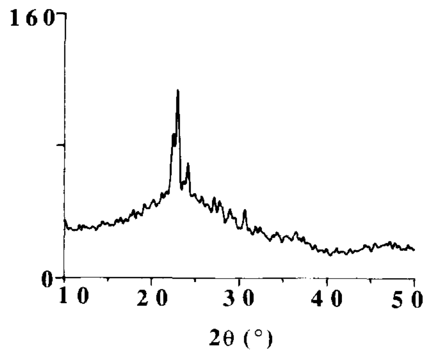

FIG. 8. XRD spectrum of the solid obtained from the E phase activated under butane/air at 390–410°C.

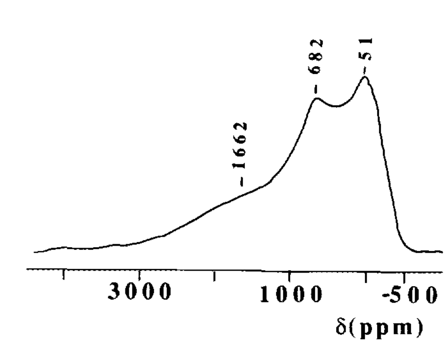

FIG. 10. ^{31}P NMR spectrum by spin-echo mapping of the solid obtained from the E phase activated under butane/air at 390–410°C.

(E_{af} and $C1_{af}$, respectively) are shown in Fig. 12 and Table 2.

DISCUSSION

Structure of the Catalyst Precursor

The X-ray diffraction pattern of the precursor (Fig. 1) is in good agreement with that previously published for $VO(H_2PO_4)_2$ (22, 24), demonstrating that this phase has been successfully synthesized. In addition to XRD characterization, we have studied the precursor structure using LRS and ^{31}P NMR by spin-echo mapping and the results given in this paper are the first reported for this material. The LRS spectrum of this phase (Fig. 2) presents a very intense band at 938 cm^{-1} and four weak bands at 903, 1110, 1148, and 1183 cm^{-1}. No bands are present below 800 cm^{-1} or above 1200 cm^{-1}. The intense signal observed at 2300 ppm on the ^{31}P NMR spectrum by spin-echo mapping (Fig. 3) agrees with the V(IV) oxidation state of this phase, since V(IV) in $VOHPO_4 \cdot 0.5H_2O$ gives a signal at 1600 ppm, while V(IV) in $(VO)_2P_2O_7$ gives a signal at 2600 ppm (23).

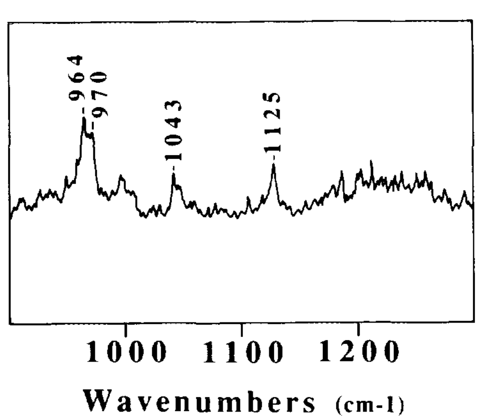

FIG. 9. LRS spectrum of the solid obtained from the E phase activated under butane/air at 390–410°C.

It is apparent that the thermal decomposition of the precursor, as evidenced by the water evolution (Fig. 4), occurs in a single transition with a very broad peak at 383°C, in agreement with previous observations (10, 20). It thus differs from the decomposition of $VOHPO_4 \cdot 0.5H_2O$, which occurs with two transitions. The single transition peak can be explained by the very different structure of $VO(H_2PO_4)_2$. According to Bordes (22), O–V–O–P–O chains are formed diagonally, each equatorial oxygen of the VO_6 octahedron being shared with one of a tetrahedron $O_2P(OH)_2$, and four tetrahedra are hydrogen-bonded by means of the two hydroxyl groups. In the perpendicular direction, the O═V ··· O═V chains are parallel to the square channels drawn by the hydrogen bonds between the chains of $O_2P(OH)_2$. As a consequence of this struc-

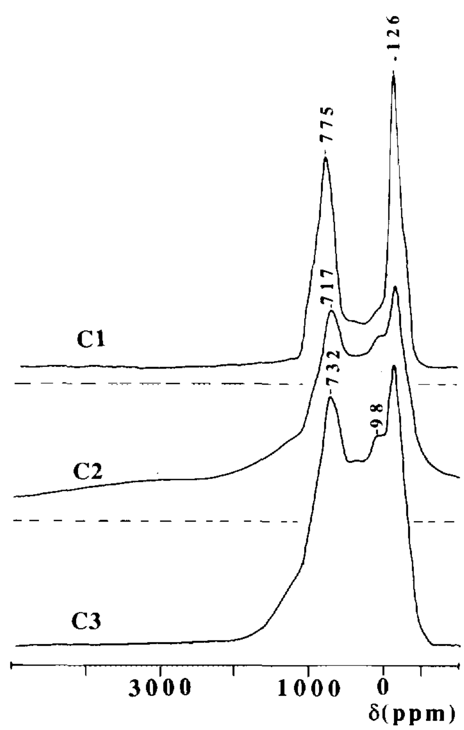

FIG. 11. ^{31}P NMR spectra by spin-echo mapping of C1, C2, and C3 catalysts after catalytic testing.

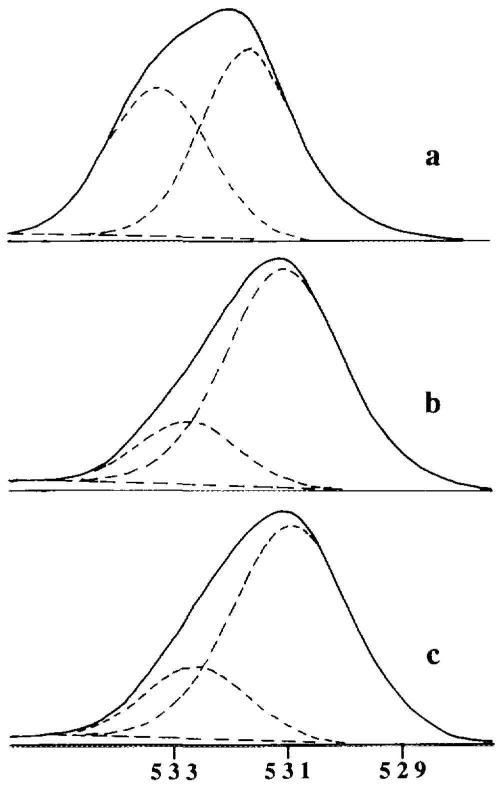

FIG. 12. XPS spectra for (a) phase E; (b) phase E after catalytic testing; (c) catalyst C1 after catalytic testing.

ture, the decomposition of $VO(H_2PO_4)_2$ affects two hydroxyl groups of the same phosphorous unit and thus explains the unique continuous transition. In contrast, $VOHPO_4 \cdot 0.5H_2O$ decomposes with two transitions due, first, to the loss of the H_2O molecule bonded to the two VO_6 units and, second, to the interaction between two P(OH) belonging to two neighboring chains (25).

Structure of the Activated Catalysts

The X-ray spectra of catalysts C1, C2, and C3 (Fig. 5) correspond to the two reference diffraction patterns of $VO(PO_3)_2$ that have been published (16, 26). C1 is highly crystalline, while C2 and C3 are poorly crystalline.

Sample C1 gives a well-resolved LRS spectrum with major characteristic bands at 961 and 972 cm^{-1} and minor bands in the 1200–1300 cm^{-1} range. The definition of this spectrum is consistent with a well-crystallized material, in agreement with the XRD pattern. C2 and C3 present much poorer spectra, typical of the poorer crystallinity of these materials.

From these studies, it is apparent that the atmosphere of calcination of $VO(H_2PO_4)_2$ strongly influences the crystallinity of the obtained $VO(PO_3)_2$ phase. This is particularly important for the treatment in the catalytic atmosphere.

The ^{31}P NMR spectra obtained by spin-echo mapping of C1, C2, and C3 (Fig. 7) show two characteristic signals at 775 and −126 ppm, in agreement with previous observations (23). The signal at −130 to −150 ppm was attributed to P atoms bonded to V^{5+} species in a strong interaction with the $VO(PO_3)_2$ structure, while the peak at 775–800 ppm was considered characteristic of P atoms bonded to the V^{4+} atoms of the $VO(PO_3)_2$ structure. The relative distribution of these two peaks depends on the atmosphere of calcination, with an increase in the contribution at −130 ppm from the nitrogen treatment (C2) or the catalytic atmosphere treatment (C3) to more oxidizing conditions (C1). From these spectra, it is also apparent that C2 and C3 appear more disorganized, with a higher contribution in the 1000–2000 ppm range, which was previously attributed to V^{4+} in poorly crystallized $(VO)_2P_2O_7$ (26). Some crystalline $(VO)_2P_2O_7$ is also observed on C2 with a small signal at 2600 ppm (23, 27). These results are therefore in agreement with the XRD and LRS characterizations.

TABLE 2

XPS Characteristics of E, E_{af}, and $C1_{af}$

	O_{1s}				$V_{2p3/2}$	P_{2p}	
Solids	E (eV)	% OH	E (eV)	% O^{2-}	E (eV)	E (eV)	P/V
E	533.0	45.1	531.4	54.9	517.1	134.1	4.00
E_{af}	533.0	18.9	531.4	81.1	517.0	133.8	3.47
$C1_{af}$	532.8	20.7	531.2	79.3	516.7	133.3	4.12

n-Butane Oxidation over Catalysts Derived from $VO(H_2PO_4)_2$

The main interest in the catalysts obtained from $VO(H_2PO_4)_2$ stems from the different distribution of the reaction products as compared to classical VPO catalysts obtained from $VOHPO_4 \cdot 0.5H_2O$.

The formation of furan with catalysts derived from $VO(H_2PO_4)_2$ together with the absence of any CO_x requires discussion, since under the same experimental conditions, furan is never detected with catalysts derived from $VOHPO_4 \cdot 0.5H_2O$. This result is not due to the varied conditions used in this study since the primary selectivity for catalysts derived from $VOHPO_4 \cdot 0.5H_2O$ is ca. 85% under our test conditions. It is notable that the intrinsic activity (IA), expressed per unit surface area, for the catalyst derived from $VO(H_2PO_4)_2$, with the exception of C1, is higher than that derived from $VOHPO_4 \cdot 0.5H_2O$. This advantage is lost when the comparison is made on the basis of catalyst mass which is a result of the low surface areas presently achieved for catalysts derived from $VO(H_2PO_4)_2$. It should also be noted that for catalysts derived from $VOHPO_4 \cdot 0.5H_2O$, maleic anhydride is mainly produced via the direct oxidation of *n*-butane and the alternative route via furan is a secondary pathway (28). In the case of the $VO(H_2PO_4)_2$-derived catalyst, it is apparent that the oxidation pathway via furan is now dominant. The results of the present study confirm the work of Morishige *et al.* (21). They also indicate that a new route of maleic anhydride synthesis without the formation of carbon oxides could be achieved with a phosphorus-rich surface. The use of catalysts based on the phosphorus-rich $VO(H_2PO_4)_2$ should be of great significance for industry if the preparation of catalysts with higher surface areas can be achieved.

Structure of the Final Catalysts

The direct activation of the E phase under 1.5% *n*-butane/air gives a poorly crystallized material in comparison with the calcination of the E phase under the same atmosphere but at a higher temperature (conditions of synthesis of catalyst C3). This is shown both by the XRD pattern (Fig. 8) with a broad signal observed between 20° and 30° (2Θ) and from the spectrum of ^{31}P NMR by spin-echo mapping (Fig. 10). In this spectrum a higher contribution can be observed in the 1000–2000-ppm range, which is indicative of the presence of disordered P environment that has been noted previously in the spectra of disorganized $(VO)_2P_2O_7$. However, there is no supporting LRS or XRD evidence for the formation of $(VO)_2P_2O_7$ as a distinct material in this catalyst sample.

No particular modifications are observed in the ^{31}P NMR by spin-echo mapping spectra of catalysts C1, C2, and C3 after catalytic testing (compare Figs. 7 and 11). This shows that the distribution of the different V^{4+} and V^{5+} species is the same before and after the test. However, a decrease in the 1000–2000-ppm contribution is apparent, which shows that the catalytic reaction has favored the crystallization of the materials.

The O_{1s} XPS spectra (Fig. 12) of the three solids can be decomposed in two peaks, one at 531.4 eV, assigned to O^{2-} of the oxide, and a second at 533.0 eV, assigned to OH groups (29–31). No surface carbonate could be considered in the O_{1s} band since the carbonate C_{1s} peak was absent within 289.2–289.6 eV (32). The presence of the 531.4 eV (O^{2-}) and 533.0 eV (OH) peaks is a common feature of the three solids, which is never observed on $(VO)_2P_2O_7$. If the presence of hydroxyl groups is normal on $VO(H_2PO_4)_2$ (E phase), it is noteworthy that OH groups are also present on $VO(PO_3)_2$ (E_{af} and $C1_{af}$) whatever the atmosphere of calcination. As observed for VPO catalysts by many authors (10–14), a surface phosphorus enrichment is also shown by XPS on the three solids (Table 2). While the chemical analysis gave a P/V ratio of 2 for the E phase, the surface P/V ratios as measured by XPS were two times higher than the bulk P/V values. This result can be used to explain the specific behavior of these catalysts.

Comments on the Specificity of the Catalysts

The absence of CO and CO_2 and the formation of furan together with maleic anhydride in the reaction products on catalysts derived from the $VO(H_2PO_4)_2$ precursor, are quite original and must be discussed in connection with previously published results on the VPO system.

In the selective oxidation of *n*-butane and butadiene to maleic anhydride, the formation of furan as a by-product has been observed (28, 33). An increase in P/V enhances the ratio between the furan and MA yields at similar conversions (33). A specific role has been considered for the phosphorus centers in the mechanism of *n*-butane oxidation and in the architecture of the active site (34–36). It is considered that the excess phosphorus isolates the VO clusters and serves "as diffusion barriers to prevent excess oxygen from reaching the surface bound intermediates" (35).

It was observed that, by controlling the availability of O_2, it was possible to maximize the formation of furan from butadiene, obtaining very high selectivity to furan (2). Transient experiments using the TAP reactor enabled Centi and co-workers to propose the existence of two types of oxygen sites on VPO (34, 36):

(i) activated species (O*) formed by strong chemisorption of the electrophilic dioxygen molecule and responsible for furan oxidation and butane activation.

(ii) surface lattice oxygen (O_{sl}) responsible for allylic oxydehydrogenation of the intermediate alkenes and for O insertion.

In the same experiments, using $^{18}O_2$ and monitoring the oxygen isotope distribution in the carbon dioxide formed as a function of time, it was shown that the fast process was $C^{18}O^{18}O$ formation involving chemisorbed oxygen-18, previously denoted O*.

All these data (2, 28, 33–36) can be used to explain the specificity of our $VO(PO_3)_2$ catalysts. The high surface P/V ratio with a high density of P–OH groups as observed by XPS can favor isolation of the VO clusters, but a lower density of O* sites due to the low superficial area of the materials should restrict the conversion of *n*-butane and this is observed. The intermediate furan molecule should then be easily desorbed in comparison with the classical VPO catalysts derived from the $VOHPO_4 \cdot 0.5H_2O$ precursor, for which the appropriate local superficial V–P–O structure at short-range order favors the further step of intermediate-furan oxidation which results in the formation and desorption of MA. The absence of CO and CO_2

indicates that the formation of part of CO_x on VPO catalysts derived from $VOHPO_4 \cdot 0.5H_2O$ occurs via the oxidation of the intermediate furan. This leads us to conclude that the two families of VPO catalysts (derived from $VO(H_2PO_4)_2$ and $VOHPO_4 \cdot 0.5H_2O$) should exhibit very different acid/base properties and this will be the subject of a future study.

ACKNOWLEDGMENTS

The authors are indebted to Dr. A. Tuel for the ^{31}P NMR studies by spin-echo mapping. They thank the Laboratoire de Physicochimie des Interfaces/CNRS at Ecole Centrale de Lyon where the LRS experiments have been performed. They also thank the Commission of the European Communities for financial support of this work (Contract CHRX CT92-0065).

REFERENCES

1. Varma, R. A., and Saraf, D. N., *Ind. Eng. Chem. Prod. Res. Dev.* **18,** 7 (1979).
2. Centi, G., Trifiro, F., Ebner, J. R., and Franchetti, V. M., *Chem. Rev.* **88,** 55 (1988).
3. Centi, G. (Ed.), "Vanadyl Pyrophosphate Catalysts" *Catal. Today* **16,** No. 1 (1993).
4. Hodnett, B. K., Permanne, Ph., and Delmon, B., *Appl. Catal.* **6,** 231 (1983).
5. Hodnett, B. K., and Delmon, B., *Appl. Catal.* **88,** 43 (1984).
6. Hodnett, B. K., *Catal. Rev.-Sci. Eng.* **27,** 373 (1985).
7. Moser, T. P., Wenig, R. W., and Schrader, G. L., *Appl. Catal.* **34,** 39 (1987).
8. Johnson, J. W., Johnston, D. C., Jacobson, A. J., and Brody, J. F., *J. Am. Chem. Soc.* **106,** 8123 (1984).
9. Bordes, E., Courtine, P., and Johnson, J. W., *J. Solid State Chem.* **55,** 270 (1984).
10. Garbassi, F., Bart, J., Tassinari, R., Vlaic, G., and Labarde, P., *J. Catal.* **98,** 317 (1986).
11. Satsuma, A., Hattori, A., Furuta, A., Miyamoto, A., Hattori, T., and Murakami, Y., *J. Phys. Chem.* **92,** 2275 (1988).
12. Harrouch-Batis, N., Batis, H., Ghorbel, A., Védrine, J. C., and Volta, J. C., *J. Catal.* **128,** 248 (1991).
13. Cornaglia, L. M., Caspani, C., and Lombardo, E. A., *Appl. Catal.* **74,** 15 (1991).
14. Bastians, Ph., Genet, M., Daza, L., Acosta, D., Ruiz, P., and Delmon, B. *in* "New Developments in Selective Oxidation by Heterogeneous Catalysis" (P. Ruiz and B. Delmon, Eds.) p. 267, Elsevier, Amsterdam, 1992.
15. Haas, J., Plog, C., Maunz, W., Mittag, K., Gollmer, K. D., and Klopries, B., *in* "Proceedings, 9th International Congress on Catalysis" (M. J. Philips and M. Ternan, Eds.), Vol. 4, p. 1632. Chem. Inst. of Canada, Toronto (1988).
16. Bordes, E., and Courtine, P., *J. Catal.* **57,** 236 (1979).
17. Hutchings, G. J., and Higgins, R., United Kingdom Patent 1 601 121, 1981, assigned to Imperial Chemical Industries.
18. Udovich, C. A., and Edwards, R. C., U.S. Patent 4 416 802, 1983, assigned to Standard Oil Co., Indiana.
19. Udovich, C. A., and Edwards, R. C., U.S. Patent 4 510 259, 1985, assigned to Standard Oil Co., Indiana.
20. Hutchings, G. J., *Appl. Catal.* **72,** 1 (1991).
21. Morishige, H., Tamaki, J., Miura, N., and Yamazoe, N., *Chem. Lett.*, 1513 (1990).
22. Bordes, E., *Catal. Today* **1,** 499 (1987).
23. Sananés, M. T., Tuel, A., and Volta, J. C., *J. Catal.* **145,** 251 (1994).
24. Villeneuve, G., *et al.*, *Mater. Res. Bull.* **21,** 621 (1986).
25. Bordes, E., Courtine, P., and Johnson, J. W., *J. Solid State Chem.* **55,** 270 (1984).
26. Lavrov, A., *Inorg. Mater. Engl. Trans.* **10,** 1869 (1974).
27. Sananés, M. T., Tuel, A., Hutchings, G. J., and Volta, J. C., *J. Catal.* **148,** 395 (1994).
28. Zhang-Lin, Forissier, M., Sneeden, R. P., Védrine, J. C., and Volta, J. C., *J. Catal.* **145,** 256 (1994).
29. Barr, T. L., *J. Phys. Chem.* **82,** 1801 (1978).
30. Haber, J., Stoch, J., and Ungier, L., *J. Electron. Spectrosc. Relat. Phenom.* **9,** 459 (1976).
31. Uwamino, Y., and Ishizuka, *J. Electron. Spectrosc. Relat. Phenom.* **34,** 67 (1984).
32. Stoch, J., and Gablankowska-Kubucz, *Surf. Interface Anal.* **17,** 165 (1991).
33. Centi, G., and Trifiro, F., *J. Mol. Catal.* **35,** 255 (1986).
34. Centi, G., Trifiro, F., Busca, G., Ebner, J., and Gleaves, J., *Faraday Discuss. Chem. Soc.* **87,** 215 (1989).
35. Agaskar, P. A., De Caul, L., and Grasselli, R. K., *Catal. Lett.* **23,** 330 (1994).
36. Busca, G., and Centi, G., *J. Am. Chem. Soc.* **111,** 46 (1989).